energies

MDPI

Article

Energy Management and Control of Plug-In Hybrid Electric Vehicle Charging Stations in a Grid-Connected Hybrid Power System

Sidra Mumtaz [1], Saima Ali [1], Saghir Ahmad [1], Laiq Khan [1,*], Syed Zulqadar Hassan [2] and Tariq Kamal [3]

[1] Department of Electrical Engineering, COMSATS Institute of Information Technology, Abbottabad 22060, Pakistan; sidramumtaz@ciit.net.pk (S.M.); saimaali@ciit.net.pk (S.A.); sagheer@ciit.net.pk (S.A.)

[2] Department of Power System and Its Automation, Chongqing University, Chongqing 400044, China; zulqadarhassan@outlook.com

[3] Department of Electrical and Electronics Engineering, Faculty of Engineering, Sakarya University, Serdivan/Sakarya 54050, Turkey; tariq.kamal.pk@ieee.org

* Correspondence: laiq@ciit.net.pk

Received: 13 October 2017; Accepted: 10 November 2017; Published: 21 November 2017

Abstract: The charging infrastructure plays a key role in the healthy and rapid development of the electric vehicle industry. This paper presents an energy management and control system of an electric vehicle charging station. The charging station (*CS*) is integrated to a grid-connected hybrid power system having a wind turbine maximum power point tracking (*MPPT*) controlled subsystem, photovoltaic (*PV*) *MPPT* controlled subsystem and a controlled solid oxide fuel cell with electrolyzer subsystem which are characterized as renewable energy sources. In this article, an energy management system is designed for charging and discharging of five different plug-in hybrid electric vehicles (*PHEVs*) simultaneously to fulfil the grid-to-vehicle (*G2V*), vehicle-to-grid (*V2G*), grid-to-battery storage system (*G2BSS*), battery storage system-to-grid (*BSS2G*), battery storage system-to-vehicle (*BSS2V*), vehicle-to-battery storage system (*V2BSS*) and vehicle-to-vehicle (*V2V*) charging and discharging requirements of the charging station. A simulation test-bed in Matlab/Simulink is developed to evaluate and control adaptively the *AC-DC-AC* converter of non-renewable energy source, *DC-DC* converters of the storage system, *DC-AC* grid side inverter and the converters of the *CS* using adaptive proportional-integral-derivate (*AdapPID*) control paradigm. The effectiveness of the *AdapPID* control strategy is validated through simulation results by comparing with conventional *PID* control scheme.

Keywords: renewable energy; hybrid power system; charging station; *PHEVs*; adaptive *PID*

1. Introduction

In the world today, fossil fuels are the dominant energy sources for power generation, but the depletion of fossil fuel reserves along with growing environmental concerns have been a wake-up call for finding the alternative energy sources. In the past few decades, the integration of renewable energy sources (*RES*) along with energy storage systems has been gaining a remarkable pace throughout the world. Plug-in hybrid electric vehicles (*PHEVs*) are achieving great popularity owing to the global call for clean energy [1]. The penetration of *PHEVs* in the power grid constitutes an emerging technology [2,3].

The *RES* and *PHEVs* potentially not only provide a clean and environmentally friendly, but also cost-effective energy. Among *RES*, the wind and photovoltaic (*PV*) power are considered foremost energy sources, because they are abundantly available in Nature [4,5]. The inherent issue of *RES* is their intermittent nature, therefore, the utilization of *RES* needs to incorporate energy storage systems [6]. Solid oxide fuel cells (*SOFCs*) are used as an alternative and versatile energy source [7]. *SOFCs* provide fuel flexibility, high efficiency and low emissions. The PHEV charging station (*CS*) integrated into a grid-connected hybrid power system (*HPS*) offers a bidirectional power flow between the utility grid and the *CS* [8,9]. The bidirectional power flow between utility grid and *CS* improves the *HPS* reliability [10]. However, the energy management and appropriate control for *PHEVs* charging station integrated into a grid-connected *HPS* are the potential areas of concern [11,12].

In a *CS*, the process of charging an uncertain number of *PHEVs* with varying energy demand causes a demand side management dilemma. Ultimately, the peak demand will be driven up which may cause system instability. An effective energy management strategy (*EMS*) controls the load peak [13,14]. In the literature, the main approaches reported for *EMS* are dynamic programming (*DP*) [15], predictive framework [16], meta-heuristic algorithms [17,18] and neural networks (*NNs*) [19,20]. The DP computes the global optimal solution, but the computational complexity increases rapidly with the number of states and control variables. The predictive *EMS* integrates the real-time traffic flow velocity data. It quickly generates a state-of-charge (*SOC*) trajectory for a *PHEV* to avoid a particular traffic route. However, the predictive framework is computationally complex and unable to deal with the uncertainties. Meta-heuristic algorithms do not involve derivative-based calculations and converge to a global optimum. However, these algorithms have long computation times, because an acceptable accuracy is achieved only after a large number of iterations. *NNs* are fast computing, easy to implement and intelligent decision makers, yet the accuracy of *NNs* depends upon the amount and quality of training.

PHEVs are considered a stochastic controllable load. The random nature of *PHEVs*' load has an unfavorable influence on the *HPS* reliability. The deterioration of *HPS* reliability affects the frequency regulation, spinning reserves and load voltage profile [21]. Therefore, an appropriate *PHEV* charging/discharging control strategy is necessary to improve the *HPS* reliability. There are two types of *PHEVs* charging techniques, i.e., uncoordinated or coordinated [22]. In uncoordinated charging, only unidirectional power flow takes place. The *PHEVs* are directly charged from the grid until their maximum *SOC* limit. However, uncoordinated charging increases the load at peak demand hours which leads to grid instability and power quality issues. The coordinated charging is characterized by bidirectional power flow which is used for charging of *PHEVs* and providing supplementary power back to the grid. The coordinated charging approach offers a number of advantages which include reduction in peak demand [23], minimization of the *HPS* operational cost [24], improvement of frequency regulation [25] and increase in the *HPS* reliability [26].

In the literature, numerous conventional techniques are used to control charging/discharging of *PHEVs* in a *HPS*. These conventional techniques involve quadratic programming and dynamic programming [27], mixed integer programming [24], linear programming [28] and proportional-integral (*PI*) control [29]. However, these conventional control systems are designed for a certain operating state and are not capable to adopt to a fluctuating environment. In case of large excursions, the system variables may go out of bound and result in system instability. Adaptive control is magnificently used to solve nonlinear and time varying uncertain control problems. Adaptive control is preferred over conventional control, because adaptive control is capable of online dealing with system nonlinearities, uncertainties and variations. A hybrid particle swarm optimization-based adaptive NeuroFuzzy system had used to control the power flow of vehicle-to-grid (*V2G*) and grid-to-vehicle (*G2V*) [30]. However, the proposed control system was complex and had large computation time. The double layered self-organized adaptive charging strategy had used for *PHEV* charging/discharging [31]. However, in the proposed model only the local load was considered in spite of the entire power grid.

In this article, an adaptive proportional-integral-derivate (*AdapPID*) control paradigm is proposed for charging/discharging of *PHEVs* in a *CS* integrated to a grid-connected *HPS* having a wind turbine maximum power point tracking (*MPPT*) controlled subsystem, a *PV MPPT* controlled subsystem and a controlled *SOFC* with electrolyzer subsystem. The overall power flow between *PHEVs*, *CS* and grid-connected *HPS* is managed by an energy management system.

The primary contributions of this research work are:

- To develop a simulation test-bed in Matlab/Simulink in which a *CS* is integrated to a grid-connected *HPS* having a wind turbine *MPPT* controlled subsystem, photovoltaic *MPPT* controlled subsystem and controlled *SOFC* with electrolyzer subsystem.
- To design an EMS for optimal power flow between five different *PHEVs*, *CS* and grid based on seven different scenarios which include *G2V*, *V2G*, grid-to-battery storage system (*G2BSS*), battery storage system-to-grid (*BSS2G*), battery storage system-to-vehicle (*BSS2V*), vehicle-to-battery storage system (*V2BSS*) and vehicle-to-vehicle (*V2V*).
- To design an adaptive control paradigm for a non-renewable energy source (micro-turbine), storage system (battery and super-capacitor), grid side inverter and the charging station (*CS* converter, battery storage system (*BSS*), *PHEVs*).

The rest of the paper is organized into four main sections: Section 2 presents the system description and problem formulation. Section 3 gives the details of the *EMS* for *CS* integrated to a grid-connected *HPS*. Simulation results are discussed in Section 4. Section 5 concludes the outcomes of this research work.

2. System Description and Problem Formulation

The *CS* shown in Figure 1 is integrated to a grid-connected *HPS* via an *AC* bus. Figure 1 represents the proposed charging station (*CS*) which consists of five different *PHEVs* and *BSS*. All the five *PHEVs* and *BSS* have a buck-boost converter and a voltage regulator. The buck-boost converter is controlled by two *AdapPID* controllers. One *AdapPID* is used in buck mode and other in boost mode. The voltage regulator is also controlled by *AdapPID*. The *CS* is connected to *AC* bus of *HPS* via *DC-AC* converter. The *DC-AC* converter is also controlled by *AdapPID*. The detail of the stated *HPS* which consists of renewable, non-renewable energy sources (micro-turbine (*MT*)), storage system (battery and super-capacitor (*SC*)), utility grid and *CS* is given in [4]. In the *HPS*, there are two types of loads which are connected to *AC* bus. One is the residential load (P_L) and other is the *CS* load (P_{CS}). The power balance equations for the residential and charging station loads are:

$$\Delta P_L(k) = +P_{ES}(k) + P_{Grid}(k) \tag{1}$$

$$\Delta P_{CS}(k) = +P_{CS-BSS}(k) + \sum_{i=1}^{N} P_{PHEV}^{\,i}(k) + P_{Grid}(k) \tag{2}$$

where N = 1, 2, . . . , 5 is the number of *PHEVs*. The load power, P_L is provided by all renewable, non-renewable energy sources and also by the utility grid. The $P_{ES}(k)$ is the power delivered by all renewable and non-renewable energy sources. The charging station power, $P_{CS}(k)$ is provided by charging station *BSS* ($P_{C-BSS}(k)$), *PHEVs* ($P_{PHEVs}(k)$) and from the grid ($P_{Grid}(k)$).

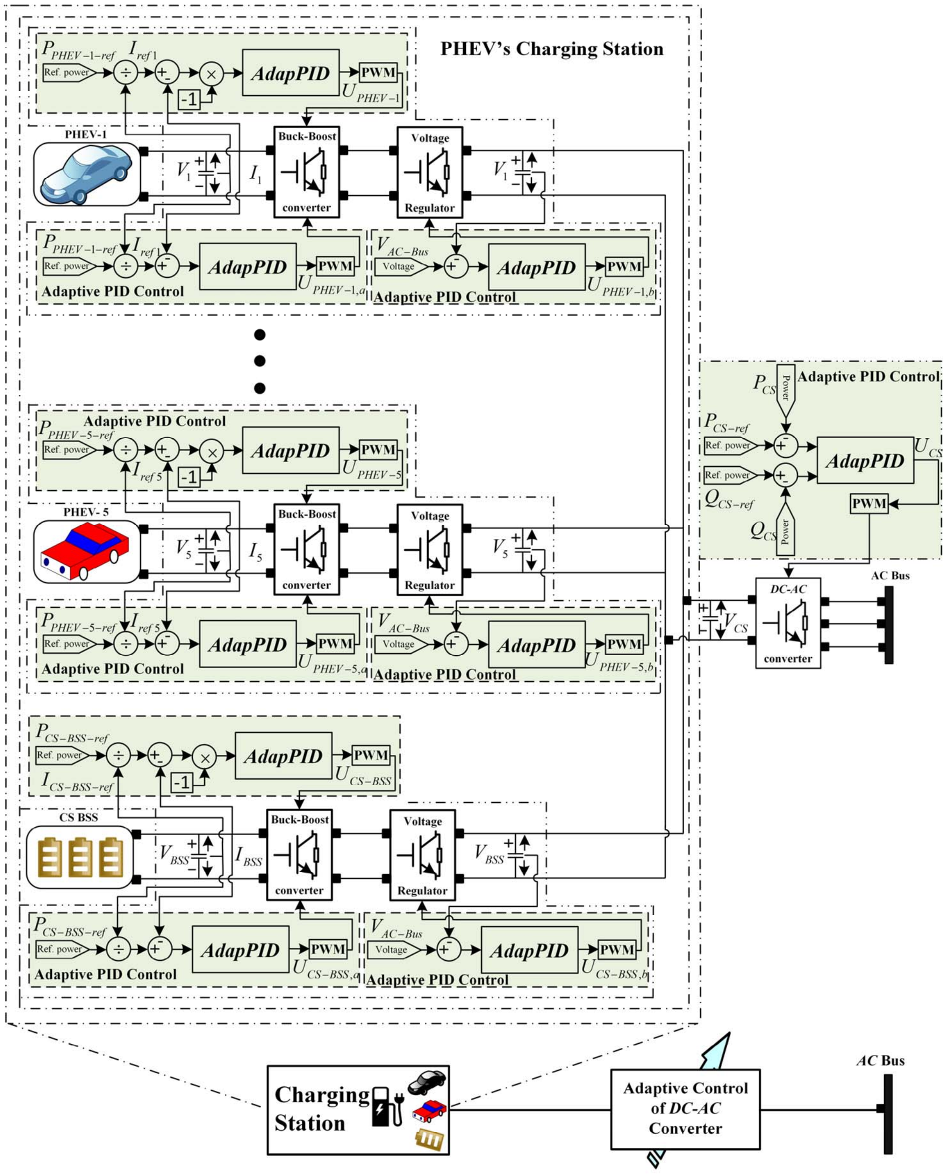

Figure 1. *PHEVs* charging station.

2.1. Problem Formulation

The nonlinear *HPS* with renewable energy sources, non-renewable energy sources, storage system, and *CS* is mathematically described as:

$$\begin{bmatrix} \hat{y}_{RES}(k) \\ y_{NRES}(k) \\ y_{SS}(k) \\ y_{GInv}(k) \\ y_{CS}(k) \end{bmatrix} = \begin{bmatrix} f_{NF-RES}(\Omega(k)) & 0 & 0 & 0 & 0 \\ 0 & f_{NRES}(x(k)) & 0 & 0 & 0 \\ 0 & 0 & f_{SS}(x(k)) & 0 & 0 \\ 0 & 0 & 0 & f_{GInv}(x(k)) & 0 \\ 0 & 0 & 0 & 0 & f_{CS}(x(k)) \end{bmatrix} \quad (3)$$

where $\hat{y}_{RES}(k) = f_{NF-RES}(\Omega(k))$ represents the auto-regression NeuroFuzzy model of the nonlinear *RES* which includes variable speed wind-turbine (*WT*), *PV* and *SOFC*. $y_{RES} = f_{NRES}(x(k))$ represents the non-linear model of non-renewable energy sources (*NRES*) which includes micro-turbines. $y_{SS} = f_{SS}(x(k))$ represents the nonlinear model of the storage system (*SS*) which includes battery and super-capacitor. $y_{GInv}(k) = f_{GInv}(x(k))$ represents the non-linear model of the grid side inverter (*GInv*) and $y_{CS}(k) = f_{CS}(x(k))$ represents the non-linear model of the *PHEVs* charging station. Also:

$$\hat{y}_{RES}(k) = [\hat{y}_{NF-WT}(k) \quad \hat{y}_{NF-PV}(k) \quad \hat{y}_{NF-SOFC}(k)]^T \tag{4}$$

where $\hat{y}_{NF-WT}(k)$, $\hat{y}_{NF-PV}(k)$ and $\hat{y}_{NF-SOFC}(k)$ are identified models of *WT*, *PV* and *SOFC* [4]. Similarly:

$$y_{NRES}(k) = [y_{MT}(k)] \tag{5}$$

$$y_{SS}(k) = [y_{BAT}(k) \quad y_{SC}(k)]^T \tag{6}$$

$$y_{GInv}(k) = [y_{GInv}(k)] \tag{7}$$

$$y_{CS}(k) = [y_{CS-Inv}(k) \quad y_{CS-BSS}(k) \quad y_{\substack{i\\PHEVs}}(k)]^T \tag{8}$$

where $i = 1, 2, \ldots, 5$.

$$f_{NF-RES}(\Omega(k)) = [f_{NF-WT}(\Omega(k)) \quad f_{NF-PV}(\Omega(k)) \quad f_{NF-SOFC}(\Omega(k))]^T \tag{9}$$

$$f_{NRES}(x(k)) = [f_{MT}(x(k))] \tag{10}$$

$$f_{SS}(x(k)) = [f_{BAT}(x(k)) \quad f_{SC}(x(k))]^T \tag{11}$$

$$f_{GInv}(x(k)) = [f_{GInv}(x(k))] \tag{12}$$

$$f_{CS}(x(k)) = [f_{CS-Inv}(x(k)) \quad f_{CS-BSS}(x(k)) \quad f_{\substack{i\\PHEVs}}(x(k))]^T \tag{13}$$

where $\Omega(k) = [y(k-1), \ldots, y(k-n), u(k), u(k-1), \ldots, u(k-m)]$ and $x(k) = [I_{MT}(k), I_{BAT}(k), I_{SC}(k), I_{GInv}(k), I_{CS-Inv}(k), I_{CS-BSS}(k), I_{PHEVs}(k), V_{MT}(k), V_{BAT}(k), V_{SC}(k), V_{GInv}(k), V_{CS-Inv}(k), V_{CS-BSS}(k), V_{PHEVs}(k)]^T$. The $\hat{y}_{NF-WT}(k)$ gives predictive output at time step k for a single-input-single-output (*SISO*) variable speed wind-turbine (*VSWT*) system. $\hat{y}_{NF-PV}(k)$ gives the predictive output at time step k for a *SISO PV* system. $\hat{y}_{NF-SOFC}(k)$ gives the predictive output at time step k for a *SISO SOFC* system. The nonlinear dynamic models for the *VSWT* system, *PV* system and *SOFC* system can be captured online if:

$$\lim_{t\to\infty} \Xi_{Ide} = \lim_{t\to\infty} \begin{bmatrix} y_{NF-WT}(k) - \hat{y}_{NF-WT}(k) \\ y_{NF-PV}(k) - \hat{y}_{NF-PV}(k) \\ y_{NF-SOFC}(k) - \hat{y}_{NF-SOFC}(k) \end{bmatrix} \Rightarrow \varepsilon_{Ide} \tag{14}$$

The control problem is to find an adaptive control law for *RES*, *NRES*, *SS*, *GInv* and *CS* given in Equation (3) as follows:

$$\begin{bmatrix} U_{NF-RES}(k) \\ U_{PID-NRES}(k) \\ U_{PID-SS}(k) \\ U_{PID-GInv}(k) \\ U_{PID-CS}(k) \end{bmatrix} = \begin{bmatrix} g_{NF-RES}(\hat{y}_{RES}(k), y_{RES-ref}(k)) \\ g_{PID-NRES}(y_{NRES}(k), y_{NRES-ref}(k)) \\ g_{PID-SS}(y_{SS}(k), y_{SS-ref}(k)) \\ g_{PID-GInv}(y_{GInv}(k), y_{GInv-ref}(k)) \\ g_{PID-CS}(y_{CS}(k), y_{CS-ref}(k)) \end{bmatrix} \tag{15}$$

Equation (15) is used to track the trajectories for the *RES*, *NRES*, *SS*, *GInv*, *CS* for all $t \in [0, \infty]$ as:

$$\lim_{t\to\infty} \Xi_{RES} = \lim_{t\to\infty} \begin{bmatrix} y_{NF-WT}(k) - y_{NF-WT-ref}(k) \\ y_{NF-PV}(k) - y_{NF-PV-ref}(k) \\ y_{NF-SOFC}(k) - y_{NF-SOFC-ref}(k) \end{bmatrix} \Rightarrow \varepsilon_{RES} \tag{16}$$

$$\lim_{t\to\infty} \Xi_{NRES} = \lim_{t\to\infty} \left[y_{NRES}(k) - y_{NRES-ref}(k) \right] \Rightarrow \varepsilon_{NRES} \tag{17}$$

$$\lim_{t\to\infty} \Xi_{SS} = \lim_{t\to\infty} \left[y_{SS}(k) - y_{SS-ref}(k) \right] \Rightarrow \varepsilon_{SS} \tag{18}$$

$$\lim_{t\to\infty} \Xi_{GInv} = \lim_{t\to\infty} \left[y_{GInv}(k) - y_{GInv-ref}(k) \right] \Rightarrow \varepsilon_{GInv} \tag{19}$$

$$\lim_{t\to\infty} \Xi_{CS} = \lim_{t\to\infty} \left[y_{CS}(k) - y_{CS-ref}(k) \right] \Rightarrow \varepsilon_{CS} \tag{20}$$

where $\varepsilon_{RES}, \varepsilon_{NRES}, \varepsilon_{SS}, \varepsilon_{GInv}, \varepsilon_{CS}$ are the small tracking errors:

$$y_{NRES}(k) = [y_{MT}(k)] = [P_{MT}(k)] \tag{21}$$

$$y_{NRES-ref}(k) = \left[y_{MT-ref}(k) \right] = \left[P_{MT-ref}(k) \right] \tag{22}$$

$$y_{SS}(k) = [y_{BAT}(k), y_{SC}(k)]^T = [P_{BAT}(k), P_{SC}(k)]^T \tag{23}$$

$$y_{SS-ref}(k) = \left[y_{BAT-ref}(k), y_{SC-ref}(k) \right]^T = \left[P_{BAT-ref}(k), P_{SC-ref}(k) \right]^T \tag{24}$$

$$y_{GInv}(k) = [P_{GInv}(k)] \tag{25}$$

$$y_{GInv-ref}(k) = \left[P_{GInv-ref}(k) \right] \tag{26}$$

$$y_{CS}(k) = \left[y_{CS-Inv}(k), y_{CS-BSS}(k), y_{\underset{PHEVs}{i}}(k) \right]^T = \left[P_{CS-Inv}(k), P_{CS-BSS}(k), P_{\underset{PHEVs}{i}}(k) \right]^T \tag{27}$$

$$\begin{aligned} y_{CS-ref}(k) &= \left[y_{CS-Inv-ref}(k), y_{CS-BSS-ref}(k), y_{\underset{PHEVs-ref}{i}}(k) \right]^T \\ &= \left[P_{CS-Inv-ref}(k), P_{CS-BSS-ref}(k), P_{\underset{PHEVs-ref}{i}}(k) \right]^T \end{aligned} \tag{28}$$

Similarly:

$$U_{NF-RES}(k) = [U_{NF-WT}(k) \quad U_{NF-PV}(k) \quad U_{NF-SOFC}(k)]^T \tag{29}$$

$$U_{PID-NRES}(k) = [U_{PID-NRES}(k)] \tag{30}$$

$$U_{PID-SS}(k) = [U_{PID-BAT}(k) \quad U_{PID-SC}(k)]^T \tag{31}$$

$$U_{PID-GInv}(k) = [U_{PID-GInv}(k)] \tag{32}$$

$$U_{PID-CS}(k) = [U_{PID-CS-Inv}(k) \quad U_{PID-CS-BSS}(k) \quad U_{\underset{PID-PHEVs}{i}}(k)]^T \tag{33}$$

The equation for $U_{NF-RES}(k)$ has been solved in [4].

2.2. Adaptive PID Control System Design

The adaptive control law $U_{SAdapPID}(k) \in [U_{PID-NRES}(k), U_{PID-SS}(k), U_{PID-GInv}(k), U_{PID-CS}(k)]$ to track the trajectories $y_{NRES-ref}(k), y_{SS-ref}(k), y_{GInv-ref}(k), y_{CS-ref}(k)$ is given as:

$$U_{AdapPID}(k) = K_{P-Adap}(k)e(k) + K_{I-Adap}(k)\int (e(k))dt + K_{D-Adap}(k)\frac{d(e(k))}{dt} \tag{34}$$

where $K_{P-Adap} \in [K_{P-Adap-NRES}, K_{P-Adap-SS}, K_{P-Adap-GInv}, K_{P-Adap-CS}]$, $K_{I-Adap} \in [K_{I-Adap-NRES}, K_{I-Adap-SS}, K_{I-Adap-GInv}, K_{I-Adap-CS}]$ and $K_{D-Adap} \in [K_{D-Adap-NRES}, K_{D-Adap-SS}, K_{D-Adap-GInv}, K_{D-Adap-CS}]$ are proportional, integral and derivative constants. The cost function for achieving the adaptive control law to solve the tracking problem for *NRES*, *SS*, *GInv* and *CS* is given as:

$$\min \downarrow J(k) = \frac{1}{2}\left[J_{NRES}^2(k), J_{SS}^2(k), J_{GInv}^2(k), J_{CS}^2(k) \right] \tag{35}$$

Subject to:

$$\begin{cases} NRES \Rightarrow & \begin{cases} K_{P-Adap-MT,\min} \leq K_{P-Adap-MT} \leq K_{P-Adap-MT,\max} \\ K_{I-Adap-MT,\min} \leq K_{I-Adap-MT} \leq K_{I-Adap-MT,\max} \\ K_{D-Adap-MT,\min} \leq K_{D-Adap-MT} \leq K_{D-Adap-MT,\max} \end{cases} \\ SS \Rightarrow & \begin{cases} K_{P-Adap-BAT,\min} \leq K_{P-Adap-BAT} \leq K_{P-Adap-BAT,\max} \\ K_{I-Adap-BAT,\min} \leq K_{I-Adap-BAT} \leq K_{I-Adap-BAT,\max} \\ K_{D-Adap-BAT,\min} \leq K_{D-Adap-BAT} \leq K_{D-Adap-BAT,\max} \\ K_{P-Adap-SC,\min} \leq K_{P-Adap-SC} \leq K_{P-Adap-SC,\max} \\ K_{I-Adap-SC,\min} \leq K_{I-Adap-SC} \leq K_{I-Adap-SC,\max} \\ K_{D-Adap-SC,\min} \leq K_{D-Adap-SC} \leq K_{D-Adap-SC,\max} \end{cases} \\ GInv \Rightarrow & \begin{cases} K_{P-Adap-GInv,\min} \leq K_{P-Adap-GInv} \leq K_{P-Adap-GInv,\max} \\ K_{I-Adap-GInv,\min} \leq K_{I-Adap-GInv} \leq K_{I-Adap-GInv,\max} \\ K_{D-Adap-GInv,\min} \leq K_{D-Adap-GInv} \leq K_{D-Adap-GInv,\max} \end{cases} \\ CS \Rightarrow & \begin{cases} K_{P-Adap-CS-Inv,\min} \leq K_{P-Adap-CS-Inv} \leq K_{P-Adap-CS-Inv,\max} \\ K_{I-Adap-CS-Inv,\min} \leq K_{I-Adap-CS-Inv} \leq K_{I-Adap-CS-Inv,\max} \\ K_{D-Adap-CS-Inv,\min} \leq K_{D-Adap-CS-Inv} \leq K_{D-AdapCS-Inv,\max} \\ K_{P-Adap-CS-BSS,\min} \leq K_{P-Adap-CS-BSS} \leq K_{P-Adap-CS-BSS,\max} \\ K_{I-Adap-CS-BSS,\min} \leq K_{I-Adap-CS-BSS} \leq K_{I-Adap-CS-BSS,\max} \\ K_{D-Adap-CS-BSS,\min} \leq K_{D-Adap-CS-BSS} \leq K_{D-Adap-CS-BSS,\max} \\ K_{P-Adap-PHEVs^{i},\min} \leq K_{P-Adap-PHEVs^{i}} \leq K_{P-Adap-PHEVs^{i},\max} \\ K_{I-Adap-PHEVs^{i},\min} \leq K_{I-Adap-PHEVs^{i}} \leq K_{I-Adap-PHEVs^{i},\max} \\ K_{D-Adap-PHEVs^{i},\min} \leq K_{D-Adap-PHEVs^{i}} \leq K_{D-Adap-PHEVs^{i},\max} \end{cases} \end{cases}$$

where:

$$J_{NRES}(k) = P_{NRES}(k) - P_{NRES-ref}(k) \tag{36}$$

$$J_{SS}(k) = \begin{cases} y_{BAT}(k) - y_{BAT-ref}(k) \\ y_{SC}(k) - y_{SC-ref}(k) \end{cases} \tag{37}$$

$$J_{GInv}(k) = y_{GInv}(k) - y_{GInv-ref}(k) \tag{38}$$

$$J_{CS}(k) = \begin{cases} y_{CS-Inv}(k) - y_{CS-Inv-ref}(k) \\ y_{CS-BSS}(k) - y_{CS-BSS-ref}(k) \\ y_{PHEVs^{i}}(k) - y_{PHEVs-ref^{i}}(k) \end{cases} \tag{39}$$

The generalized update law for the parameter $K_{Adap} \in \left\{K_{P-Adap}, K_{I-Adap}, K_{D-Adap}\right\}$ is given as:

$$K_{Adap}(k+1) = K_{Adap}(k) + \alpha_{Adap}\frac{\partial J(k)}{\partial K_{Adap}(k)} \tag{40}$$

where α_{Adap} is the learning rate, i.e., $0 < \alpha_{Adap} < 1$. The gradient descent algorithm is used to update the K_{Adap} as follows:

$$\frac{\partial J(k)}{\partial K_{Adap}(k)} = -\frac{\partial J(k)}{\partial y(k)}\frac{\partial y(k)}{\partial U_{AdapPID}(k)}\frac{\partial U_{AdapPID}(k)}{\partial K_{Adap}(k)} \tag{41}$$

where $y(k) = [y_{NRES}(k), y_{SS}(k), y_{GInv}(k), y_{CS}(k)]$, $\frac{\partial J(k)}{\partial y(k)} = -e(k)$ and $\frac{\partial y(k)}{\partial U_{AdapPID}(k)} = 1$ [32]. The term $\frac{\partial U_{AdapPID}(k)}{\partial K_{Adap}(k)}$ which is associated with K_{P-Adap}, K_{I-Adap}, K_{D-Adap} can be calculated as $\frac{\partial U_{AdapPID}(k)}{\partial K_{P-Adap}(k)} = e(k)$, $\frac{\partial U_{AdapPID}(k)}{\partial K_{I-Adap}(k)} = \int e(k)dt$ and $\frac{\partial U_{AdapPID}(k)}{\partial K_{D-Adap}(k)} = \frac{d(e(k))}{dt}$. The error $e(k)$ is calculated as:

$$e(k) = y(k) - y_{ref}(k) \tag{42}$$

where $y_{ref}(k) = \left[y_{NRES-ref}(k), y_{SS-ref}(k), y_{GInv-ref}(k), y_{CS-ref}(k)\right]$. Therefore, the update equations for K_{P-Adap}, K_{I-Adap}, K_{D-Adap} are:

$$K_{P-Adap}(k+1) = K_{P-Adap}(k) + \alpha_{Adap}e^2(k) \tag{43}$$

$$K_{I-Adap}(k+1) = K_{I-Adap}(k) + \alpha_{Adap}e(k)\int e(k)dt \tag{44}$$

$$K_{D-Adap}(k+1) = K_{D-Adap}(k) + \alpha_{Adap}e(k)\frac{d(e(k))}{dt} \tag{45}$$

3. Energy Management System for the Charging Station

The *EMS* ensures the continuous and reliable power supply to the *CS* load, i.e., $P_{CS}(k)$. To satisfy the $P_{CS}(k)$ and enhance the *HPS* reliability, the *EMS* offers seven different modes of operation which include *G2V*, *V2G*, *G2BSS*, *BSS2G*, *BSS2V*, *V2BSS* and *V2V*. The detail of these modes are as follows:

- Mode-1: *G2V*: $V_{Grid}(k) > V_{CS}(k) \quad \& \quad SOC_{CS-BSS}(k) \leq 20\% \quad \& \quad SOC_{PHEVs}^{\;i}(k) < 90\%$

Where $V_{Grid}(k)$ is the grid voltage, $V_{CS}(k)$ is the *CS* voltage, $SOC_{CS-BSS}(k)$ is the *SOC* of *BSS* and $SOC_{PHEVs}^{\;i}(k)$ is the *SOC* of the *i*th PHEV. In this mode, the *PHEVs* are charged with the power taken from the utility grid. The *SOC* of *BSS* is less than 20%. The *PHEVs* are preferred to charge during off peak hours of the grid. The power balance equation for *G2V* mode is given as:

$$\Delta P_{CS}(k) = -\sum_{i=1}^{N} P_{PHEVs}^{\;i}(k) + P_{Grid}(k) \tag{46}$$

A '+' symbol represents the power delivered by the source and a '−' symbol represents the power absorbed by the load.

- Mode-2: *V2G*: $V_{CS}(k) > V_{Grid}(k) \quad \& \quad SOC_{CS-BSS}(k) \geq 90\% \quad \& \quad SOC_{PHEVs}^{\;i}(k) \geq 20\%$

During the peak demand hours of the grid, the *PHEVs* help to reduce the stress on the grid. The *PHEVs* are discharged and deliver the power to the utility grid via *AC* bus. The power balance equation for this mode of operation is given as:

$$\Delta P_{CS}(k) = +\sum_{i=1}^{N} P_{PHEVs}^{\;i}(k) - P_{Grid}(k) \tag{47}$$

- Mode-3: *G2BSS*: $V_{Grid}(k) > V_{CS}(k) \quad \& \quad SOC_{CS-BSS}(k) < 90\% \quad \& \quad SOC_{PHEVs}^{\;i}(k) \geq 20\%$

During this mode of operation, the grid is having off peak hours. Therefore, the utility grid delivers the power to charge the *BSS*. The power balance equation is given as follows:

$$\Delta P_{CS}(k) = -P_{CS-BSS}(k) + P_{Grid}(k) \tag{48}$$

- Mode-4: *BSS2G*: $V_{CS}(k) > V_{Grid}(k) \quad \& \quad SOC_{CS-BSS}(k) \geq 20\% \quad \& \quad SOC_{PHEVs}^{\;i}(k) \geq 20\%$

The operation of this mode is similar to *V2G* mode but the *BSS* is in discharge mode in-spite of *PHEVs*. The *BSS* also supplies the power to the utility grid during its peak demand hours. This mode has the following power balance equation.

$$\Delta P_{CS}(k) = +P_{CS-BSS}(k) - P_{Grid}(k) \tag{49}$$

- Mode-5: *BSS2V*: $V_{CS}(k) = V_{Grid}(k) \quad \& \quad SOC_{CS-BSS}(k) \geq 20\% \quad \& \quad SOC_{\underset{PHEVs}{i}}(k) < 90\%$

In this mode of operation, the utility grid is at peak demand hours. The *SOC* of *BSS* is greater than 20%. Therefore, the *PHEVs* are charged from the *BSS*. The power balance equation for this mode of operation is defined as:

$$\Delta P_{CS}(k) = +P_{CS-BSS}(k) - \sum_{i=1}^{N} P_{\underset{PHEVs}{i}}(k) \tag{50}$$

- Mode-6: *V2BSS*: $V_{CS}(k) = V_{Grid}(k) \quad \& \quad SOC_{CS-BSS}(k) < 90\% \quad \& \quad SOC_{\underset{PHEVs}{i}}(k) \geq 20\%$

In this mode, the *PHEVs* are discharged and they deliver the power to charge the *BSS*. The power balance equation is given as:

$$\Delta P_{CS}(k) = -P_{CS-BSS}(k) + \sum_{i=1}^{N} P_{\underset{PHEVs}{i}}(k) \tag{51}$$

- Mode-7: *V2V*: $V_{CS}(k) = V_{Grid}(k) \quad \& \quad SOC_{CS-BSS}(k) \leq 20\% \quad \& \quad 20\% \leq SOC_{\underset{PHEVs}{i}}(k) \leq 90\%$

During this mode of operation, the *PHEV* demand is fulfilled by another *PHEV*. The charging power of the *PHEV* is equal or greater than the discharging power of the *PHEV*. The power balance equation for *V2V* mode is given as follow:

$$\Delta P_{CS}(k) = +\sum_{i=1}^{N} P_{\underset{PHEVs}{i}}(k) - \sum_{i=1}^{N} P_{\underset{PHEVs}{i}}(k) \tag{52}$$

The flow chart for the charging station *EMS* is shown in Figure 2.

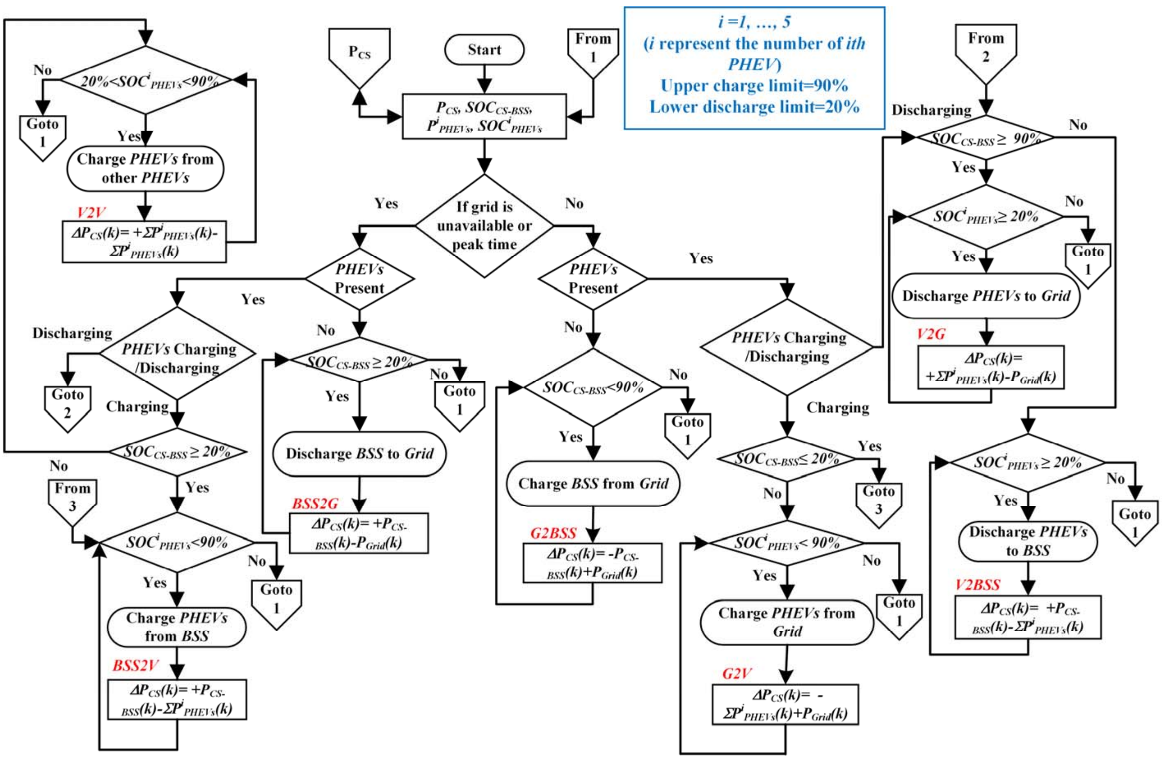

Figure 2. *EMS* flowchart.

All the seven modes of *EMS* in the *HPS* are depicted in Figure 3.

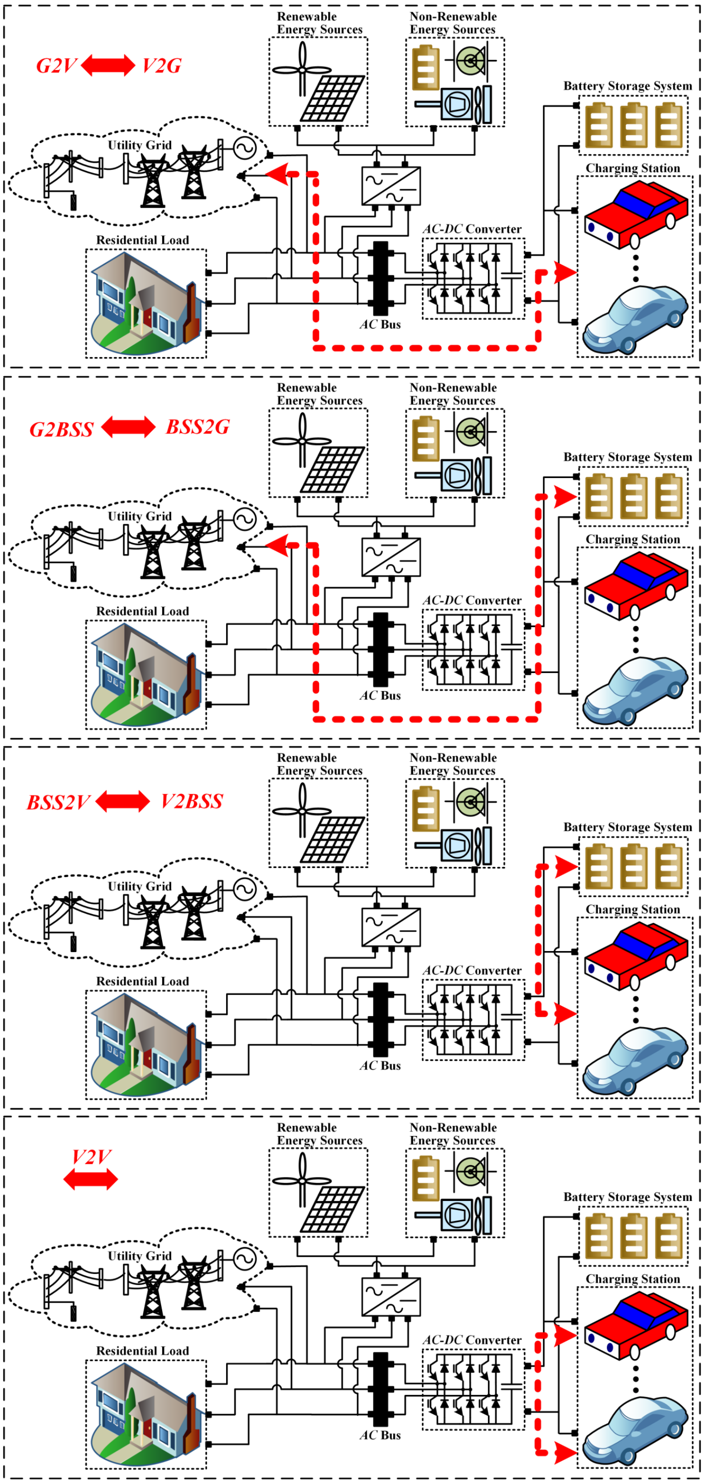

Figure 3. Modes of operation.

4. Results and Discussion

The performance of the *CS* in a grid-connected *HPS* has been evaluated with both adaptive and conventional approaches in MATLAB/Simulink R2015a (The MathWork Inc, Natick, MA, USA). The *HPS* consists of 11 kV of the grid, 100 kW of wind generation, 260 kW of *PV*, 200 kW of *SOFC*, 150 kW of the electrolyzer and 200 kVA of MT. The backup sources include battery (200 Ah) and SC (165 F). All the energy sources are modeled for the accumulative dynamic residential and charging station load. Defense Housing Authority (*DHA*), Islamabad, Pakistan, is taken as a case study. The hourly basis wind speed (m/s), irradiance (W/m^2) and ambient temperature (°C) levels are recorded by the Pakistan Meteorological Department (*PMD*). There are two types of loads in the *HPS* which are residential load and *CS* load. The residential load and *CS* load are connected to AC bus. The power to the total load (P_L + P_{CS}) is provided by all the *RES*, *NRES*, *SS*, *CS* and the utility grid via *AC* bus. The active and reactive powers of AC bus is shown in Figure 4a,b. The *AdapPID* controller adequately controls the grid inverter to track the active and reactive power reference trajectories to ensure energy balance between generation and load. The steady-state error (SSE) with *AdapPID* control is 1 kW, whereas, *PID* control has 6.68 kW. The undershoot with *AdapPID* control is 2% while the *PID* control has 66%.

The *DC-AC* converter of the *CS* is responsible for bidirectional power flow between *CS* and the utility grid. In *G2BSS*, *BSS2G*, *G2V* and *V2G* modes of operation, the *DC-AC* converter of *CS* is involved. The active and reactive powers of the *DC-AC* converter for *CS* is shown in Figure 5. During 0–2 h, the *CS* takes 50 kW power from the utility grid. This 50 kW power is used to charge the *BSS*. In time interval 4–5 h, the *CS* utilizes 70 kW power from the grid in *G2V* mode. During time intervals 11–12, 14–15 and 16–17, the *CS* delivers the power to the utility grid in *V2G* mode. In time interval 18–22 h, the *CS* delivers 30 kW power to the utility grid in *BSS2G* mode. The *AdapPID* closely tracks the active and reactive powers of *CS*.

The *AdapPID* control scheme adequately manipulates the charging station *DC-AC* inverter to track the *CS* active and reactive power reference trajectories. It results in less oscillations and SSE error as compared to conventional *PID* controller as shown in Figure 5.

The *CS* consists of five different *PHEVs* and a *BSS*. These *PHEVs* and *BSS* act as either loads or energy sources. Each *PHEV/BSS* has its own buck-boost converter. The buck mode is used to charge the *PHEV/BSS*, whereas, the boost mode is used to discharge the *PHEV/BSS*. The buck-boost converter is controlled by *AdapPID*. Based on the reference power, each buck-boost converter extracts or delivers the power to the *PHEVs*/BSS. To meet the dynamic *CS* load, the *EMS* offers seven different modes of operation which include *G2V*, *V2G*, *G2BSS*, *BSS2G*, *BSS2V*, *V2BSS* and *V2V* as shown in Figure 6.

Figure 6a represents the *BSS* power. During off peak hours of the grid, i.e., 0–2 h, the *G2BSS* mode is activated. The *BSS* is charged from the grid power. The *BSS* utilizes 50 kW power from the grid. During 11–12 h, the *BSS* is again in charge mode and the *V2BSS* mode is activated. The *PHEV-3* delivers 20 kW power to charge the *BSS* as shown in Figure 6d. For t = 13–15 h, the *BSS2V* mode is activated. During this mode of operation, the *BSS* delivers 20 kW power to *PHEV-5* as shown in Figure 6f. During 18–22 h, the *BSS2G* mode is ON, becasuse the grid is having peak demand hours and the *BSS* tries to reduce the stress on the grid. The *BSS* delivers 30 kW power to the utility grid. Figure 6b shows the power of *PHEV-1*. *PHEV-1* is charged from *PHEV-2* during 1–2 h in *V2V* mode. *PHEV-2* delivers 30 kW power to the *PHEV-1* as shown in Figure 6b,c. The *PHEV-1* is in *V2G* mode during 14–15 h as shown in Figure 6b. During this mode of operation, the *PHEV-1* delivers 20 kW power to the utility grid via *DC-AC* converter of the *CS*. Figure 6d shows the *PHEV-3* power. During 4–5 h, the *PHEV-3* is charged from the grid in *G2V* mode. The grid is having off peak hours, therefore, the *PHEV-3* utilizes 50 kW power from the grid. During 10–11 h, the *PHEV-3* delivers the power to the BSS in *V2BSS* mode.Figure 6e shows the *PHEV-4* power. The *PHEV-4* utilizes 20 kW power from the grid during 4–5 h. In this time interval, the *G2V* mode is activated. For the peak demand hours of the grid, i.e., 11–12 h, the *V2G* mode is ON. The *PHEV-4* delivers 20 kW power to the utility grid. Figure 6f shows the power of *PHEV-5*. During 13–15 h, the *BSS2V* mode is ON and the *PHEV-5* is charged from the *BSS* power. For t = 16–17 h, the *V2G* mode is activated. In this time interval, the *PHEV-5* delivers 10 kW power to the utility grid. The BSS and *PHEVs* powers are more accurately tracked with *AdapPID* as compared to *PID*, because the *AdapPID* has smaller overshoot, undershoot and SSE as shown in Figure 6. While the conventional *PID* most of the time loses tracking as shown in Figure 6a,d. Similarly, the undershoot is high with *PID* as shown in Figure 6b–e.

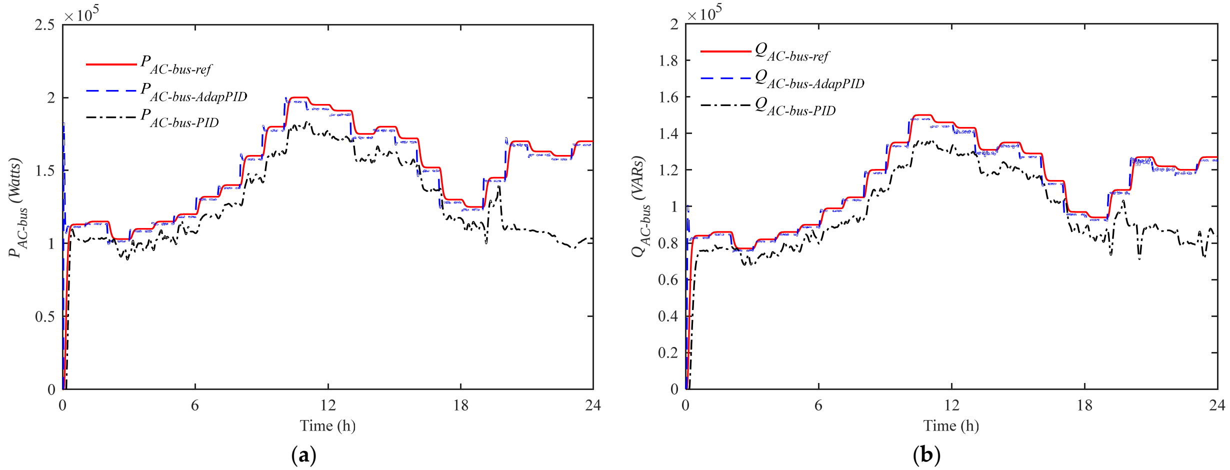

Figure 4. *AC* bus (**a**) Active power; (**b**) Reactive power.

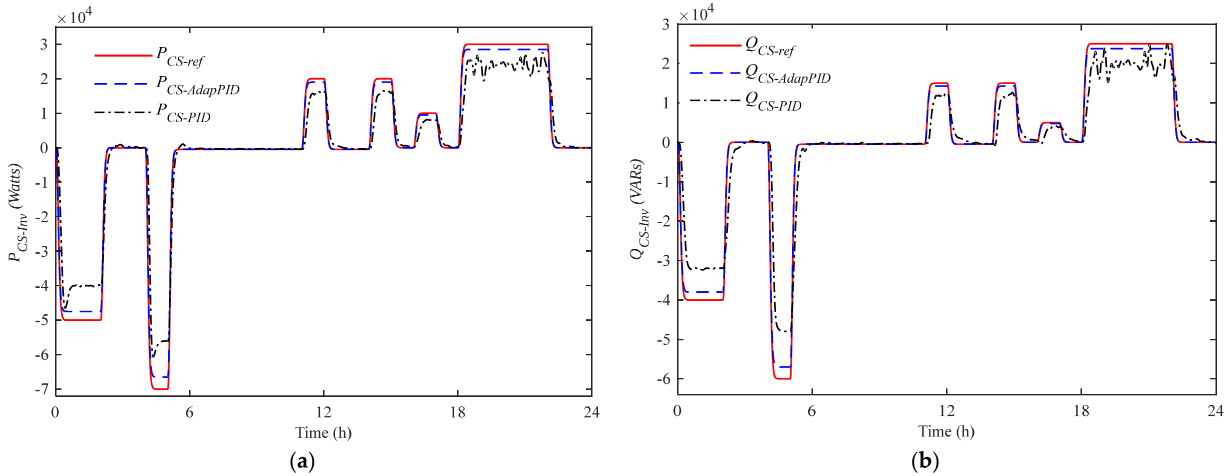

Figure 5. *CS* converter (**a**) Active power (**b**) Reactive power.

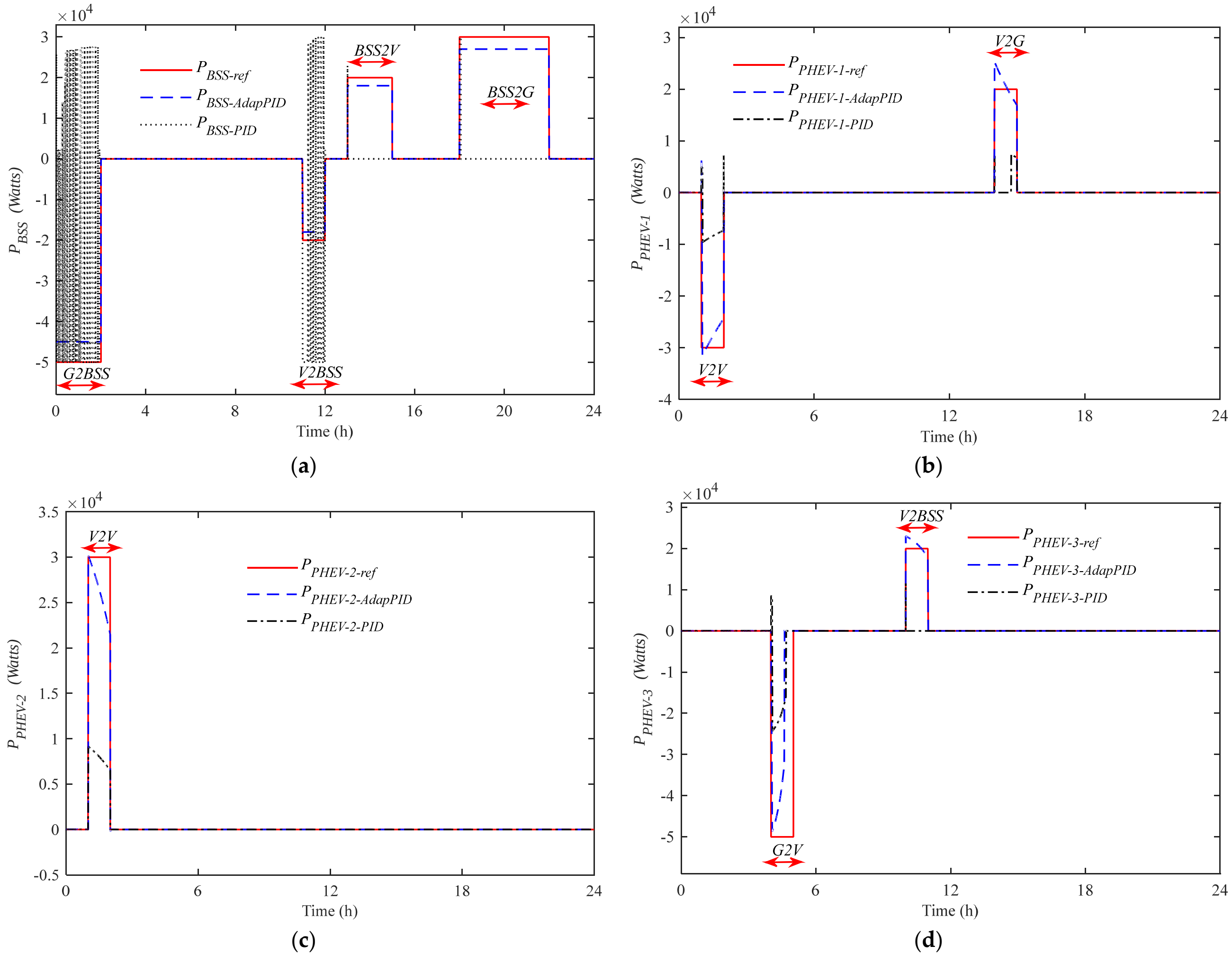

Figure 6. *Cont.*

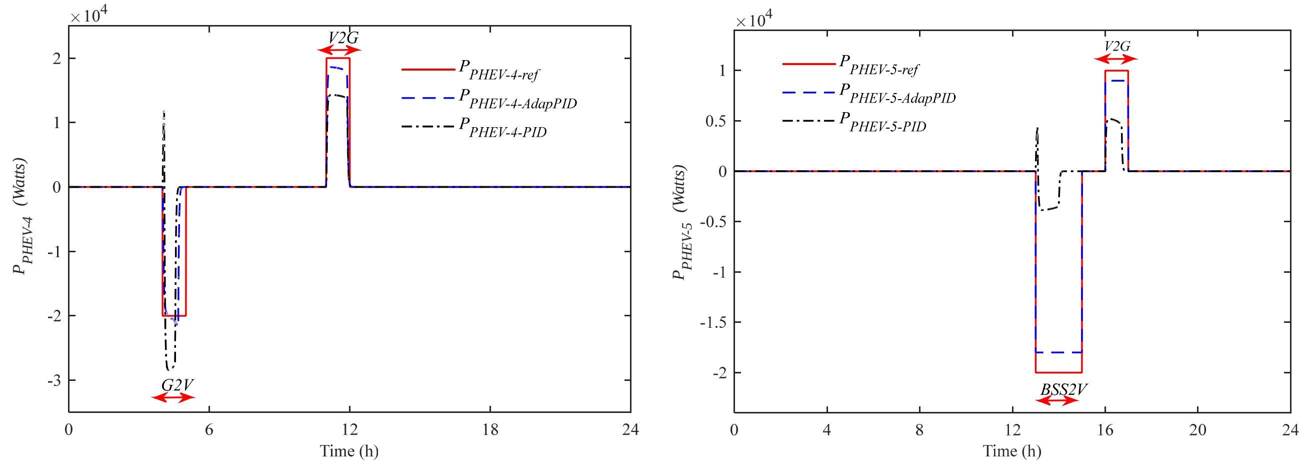

(**e**) (**f**)

Figure 6. Power of (**a**) *BSS* (**b**) *PHEV-1* (**c**) *PHEV-2* (**d**) *PHEV-3* (**e**) *PHEV-4* (**f**) *PHEV-5*.

The corresponding *SOCs* during charge/discharge mode of the BSS and *PHEVs* are shown in Figure 7. All the *PHEVs* and *BSS* are allowed to discharge and charge within 20% < *SOC* < 90%. In Figure 7a, for t = 0–2 h, the *BSS* is in charge mode and the *SOC* of the *BSS* increases from 40% to 59% with *AdapPID*. During the time interval 11–12 h, the *BSS* is again in charge mode and the *SOC* increases from 59% to 65.88%. In the next time interval, i.e., 13–15 h when the *BSS* is in discharge mode the *SOC* of *BSS* decreases from 65.88% to 58.63%. During 18–22 h, the *BSS* is again in discharge mode and the *SOC* decreases from 58.63% to 44.21%. Figure 7b represents the *SOC* for charge/discharge mode of the *PHEV-1*. During 1–2 h, the *PHEV-1* is in charge mode and the *SOC* increases from 35% to 51%.

In the time interval 14–15 h, the *PHEV-1* is discharged and the *SOC* decreases from 51% to 45.84%. The *PHEV-2* is in discharge mode during 1–2 h and the *SOC* of the vehicle decreases from 80% to 35.87% as shown in Figure 7c. The *SOC* of *PHEV-3* is shown in Figure 7d. During 4–5 h, the *PHEV-3* is in charge mode. In this time interval, the *SOC* of *PHEV-3* increases from 35% to 90%. Similarly, in interval 10–11 h, the *PHEV-3* is in discharge mode and the *SOC* decreases from 90% to 32%. Figure 7e represents the *SOC* of *PHEV-4*. During 4–5 h, the *PHEV-4* is in charge mode and the *SOC* of *PHEV-4* increases from 35% to 85%. Similarly, in interval 11–12 h, the *PHEV-4* is in discharge mode and the *SOC* decreases from 85% to 21%. Figure 7f represents the *SOC* of *PHEV-5*. During 13–15 h, the *PHEV-5* is in charge mode and the *SOC* of *PHEV-5* increases from 42% to 90%.

Similarly, in interval 16–17 h, the *PHEV-5* is in discharge mode and the *SOC* decreases from 90% to 26%. The *SOCs* of *PHEVs* are also accurately acquired with *AdapPID* as shown in Figure 7. While the conventional *PID* most of the time loses tracking as shown in Figure 7a,d.

The reference power transfer levels for *BSS* and *PHEVs* are shown in Table 1. The reference power transfer levels for *BSS* and *PHEVs* are assumed in this study. These power transaction levels are assumed to maximize the revenue. This profit is possible when all the *PHEVs* and *BSS* have access to the real-time electricity price information which varies throughout the 24 h. However, the process of deriving such schedule is not within the scope of this study.

To evaluate the *HPS* stability and power quality, different parameters are also calculated which include total harmonic distortions (*THD*) for *CS* converter current and voltage, load rms voltage, and load frequency. The *HPS* stability and power quality assumption are applied according to IEEE Std. 1547 [33]. The percentage change in *THDs* for both current and voltage is shown in Figure 8. The percentage change in load rms voltage and frequency is shown in Figure 9. The *AdapPID* controller has a flat profile as compared to *PID* controller for the percentage change in current *THD*, voltage *THD*, load rms voltage and frequency. The charging station with *AdapPID* control injects less harmonics into the *AC* bus which greatly enhances the quality of load voltage and current. It also keeps the system frequency well within the IEEE Std. 1547 [33].

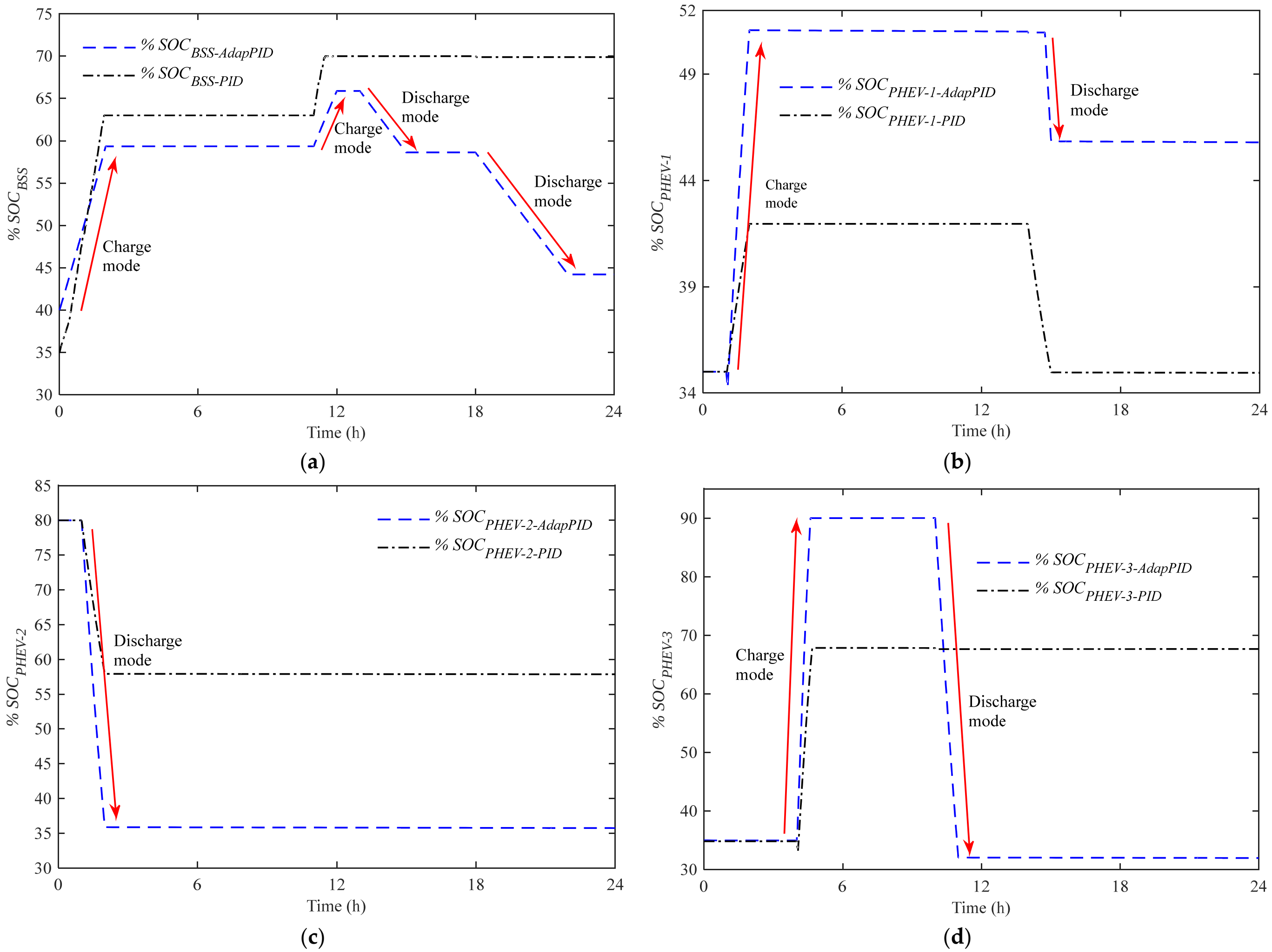

Figure 7. *Cont.*

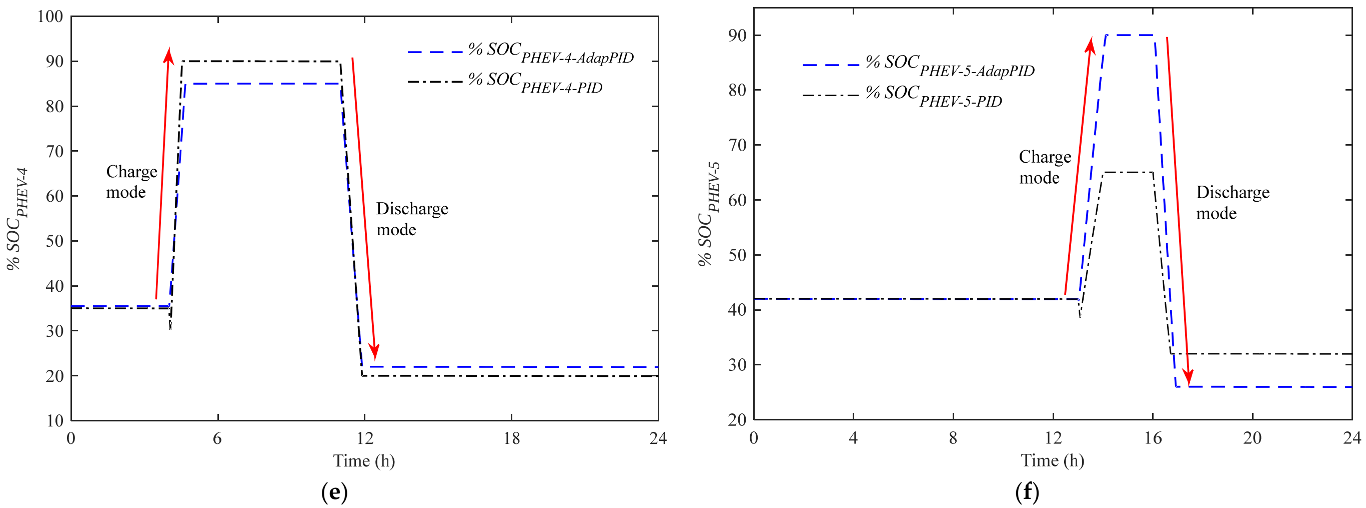

Figure 7. % *SOCs* of (**a**) *BSS* (**b**) *PHEV-1* (**c**) *PHEV-2* (**d**) *PHEV-3* (**e**) *PHEV-4* (**f**) *PHEV-5*.

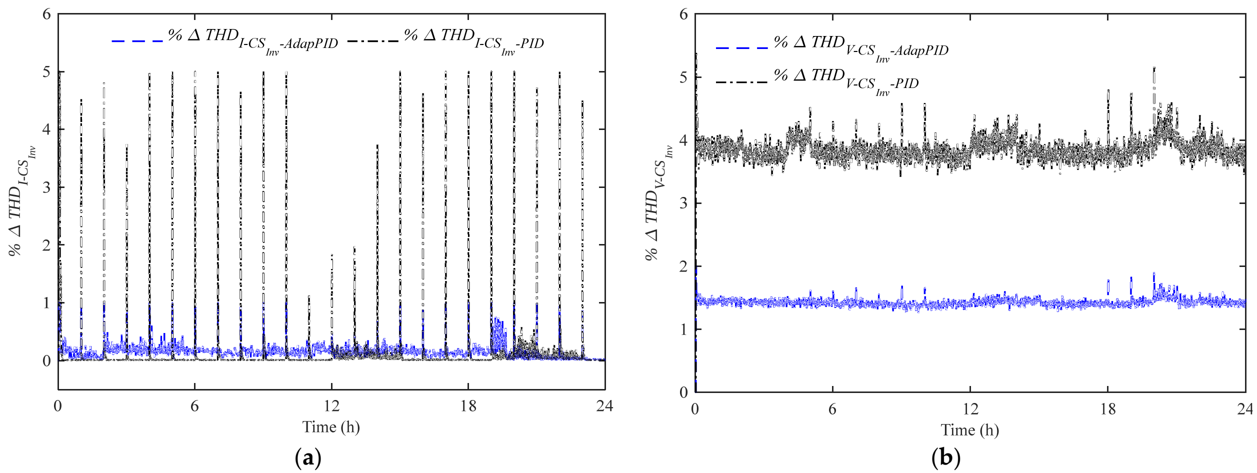

Figure 8. % change in *CS* converter (**a**) Current *THDs* (**b**) Voltage *THDs*.

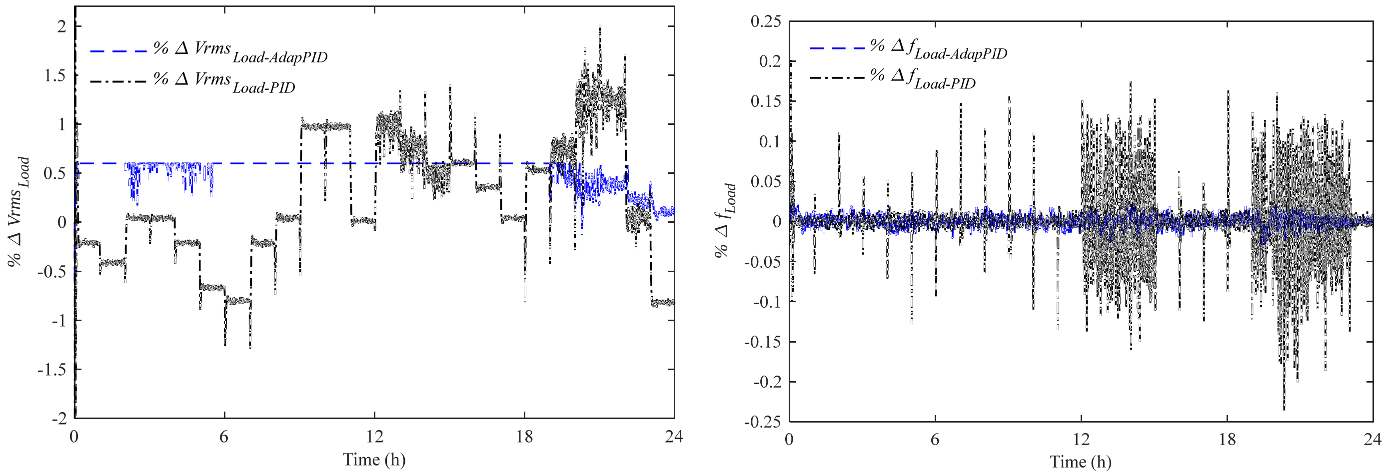

(**a**) (**b**)

Figure 9. % change in load (**a**) RMS voltage (**b**) Frequency.

Table 1. Reference power transfer levels in kW for respective vehicles and hours.

Vehicle	t_1	t_2	t_3	t_4	t_5	t_6	t_7	t_8	t_9	t_{10}	t_{11}	t_{12}	t_{13}	t_{14}	t_{15}	t_{16}	t_{17}	t_{18}	t_{19}	t_{20}	t_{21}	t_{22}	t_{23}	t_{24}
BSS	−50	−50	0	0	0	0	0	0	0	0	−20	0	+20	+20	0	0	0	+30	+30	+30	+30	0	0	0
PHEV-1	0	−30	0	0	0	0	0	0	0	0	0	0	0	+20	0	0	0	0	0	0	0	0	0	0
PHEV-2	0	+30	0	0	0	0	0	0	0	0	0	0	0	0	0	0	0	0	0	0	0	0	0	0
PHEV-3	0	0	0	−50	0	0	0	0	0	+20	0	0	0	0	0	0	0	0	0	0	0	0	0	0
PHEV-4	0	0	0	−20	0	0	0	0	0	0	+20	0	0	0	0	0	0	0	0	0	0	0	0	0
PHEV-5	0	0	0	0	0	0	0	0	0	0	0	0	−20	−20	0	+10	0	0	0	0	0	0	0	0

5. Conclusions

In this article, an energy management system and control of *PHEVs* of a charging station in a hybrid power system has been presented. The charging station consists of *DC-DC* converters for *PHEVs* and *AC-DC* converter for interfacing to AC bus. The renewable energy sources are adaptively controlled to extract maximum power. In the simulation, *G2V*, *V2G*, *G2BSS*, *BSS2G*, *BSS2V*, *V2BSS* and *V2V* operations of the charging station have been simulated. Best performance has been demonstrated in all modes of operation of charging station by adaptively controlled *DC-DC* and *AC-DC* converters. It is obvious from the results that the adaptive *PID* control system adequately tracks the demanded/delivered power by the vehicles in a charging station as compared to a conventional *PID* control scheme.

Acknowledgments: The authors received no specific funding for this work.

Author Contributions: The Sidra Mumtaz, Saima Ali, Saghir Ahmad, Laiq Khan, Syed Zulqadar Hassan and Tariq Kamal conceived and designed the experiments; Sidra Mumtaz performed the experiments; Sidra Mumtaz and Laiq Khan analyzed the data; Sidra Mumtaz, Saima Ali, Saghir Ahmad, Laiq Khan, Syed Zulqadar Hassan and Tariq Kamal contributed reagents/materials/analysis tools; Sidra Mumtaz wrote the paper.

Conflicts of Interest: The authors declare no conflict of interest.

References

1. Mohamed, A.; Salehi, V.; Ma, T.; Mohammed, O. Real-time energy management algorithm for plug-in hybrid electric vehicle charging parks involving sustainable energy. *IEEE Trans. Sustain. Energy* **2014**, *2*, 577–586. [CrossRef]
2. Su, W.; Eichi, H.; Zeng, W.; Chow, M.-Y. A survey on the electrification of transportation in a smart grid environment. *IEEE Trans. Ind. Inform.* **2012**, *1*, 1–10. [CrossRef]
3. Ashish, R.H.; Juvvanapudi, M.; Bajpai, P. Issues and solution approaches in PHEV integration to smart grid. *Renew. Sustain. Energy Rev.* **2014**, *30*, 217–229. [CrossRef]
4. Sidra, M.; Khan, L.; Ahmed, S.; Bader, R. Indirect adaptive soft computing based wavelet-embedded control paradigms for *WT/PV/SOFC* in a grid/charging station connected hybrid power system. *PLoS ONE* **2017**, *12*, e0183750. [CrossRef]
5. Syed, Z.H.; Li, H.; Kamal, T.; Arifoğlu, U.; Mumtaz, S.; Khan, K. Neuro-Fuzzy Wavelet Based Adaptive *MPPT* Algorithm for Photovoltaic Systems. *Energies* **2017**, *10*, 394. [CrossRef]
6. Sidra, M.; Khan, L. Indirect adaptive neurofuzzy Hermite wavelet based control of *PV* in a grid-connected hybrid power system. *Turk. J. Electr. Eng. Comput.* **2017**, *25*, 4341–4353. [CrossRef]
7. Sidra, M.; Khan, L. Adaptive control paradigm for photovoltaic and solid oxide fuel cell in a grid-integrated hybrid renewable energy system. *PLoS ONE* **2017**, *12*, e0173966. [CrossRef]
8. Uwakwe, U.; Mahajan, S.M. *V2G* parking lot with *PV* rooftop for capacity enhancement of a distribution system. *IEEE Trans. Sustain. Energy* **2014**, *5*, 119–127. [CrossRef]
9. Evangelos, K.; Hatziargyriou, N.D. Distributed coordination of electric vehicles providing *V2G* services. *IEEE Trans. Power Syst.* **2016**, *31*, 329–338. [CrossRef]
10. Guo, D.; Zhou, C. Potential performance analysis and future trend prediction of electric vehicle with *V2G*/V2H/V2B capability. *AIMS Energy* **2016**, *4*, 331–346. [CrossRef]
11. Hassan, H.F. Novel wind powered electric vehicle charging station with vehicle-to-grid (*V2G*) connection capability. *Energy Convers. Manag.* **2017**, *136*, 229–239. [CrossRef]
12. Preetham, P.G.; Shireen, W. *PV* powered smart charging station for *PHEVs*. *Renew. Energy* **2014**, *66*, 280–287. [CrossRef]
13. Clara, M.M.; Hu, X.; Cao, D.; Velenis, E.; Gao, B.; Wellers, M. Energy management in plug-in hybrid electric vehicles: Recent progress and a connected vehicles perspective. *IEEE Trans. Veh. Technol.* **2017**, *66*, 4534–4549. [CrossRef]
14. Morteza, M.G.; Mahmoodi, M. Optimized predictive energy management of plug-in hybrid electric vehicle based on traffic condition. *J. Clean. Prod.* **2016**, *139*, 935–948. [CrossRef]
15. Pinak, T.; Marano, V.; Rizzoni, G. Energy management for plug-in hybrid electric vehicles using equivalent consumption minimization strategy. *Int. J. Electr. Hybrid Veh.* **2010**, *2*, 329–350.

16. Chao, C.; Moura, S.J.; Hu, X.; Hedrick, K.; Sun, F. Dynamic traffic feedback data enabled energy management in plug-in hybrid electric vehicles. *IEEE Trans. Control Syst. Technol.* **2015**, *23*, 1075–1086. [CrossRef]
17. Zheng, C.; Mi, C.C.; Xu, J.; Gong, X.; You, C. Energy management for a power-split plug-in hybrid electric vehicle based on dynamic programming and neural networks. *IEEE Trans. Veh. Technol.* **2014**, *63*, 1567–1580. [CrossRef]
18. Qi, X.; Wu, G.; Boriboonsomsin, K.; Barth, M. Development and evaluation of an evolutionary algorithm-based online energy management system for plug-in hybrid electric vehicles. *IEEE Trans. Intell. Transp.* **2017**, *18*, 2181–2191. [CrossRef]
19. Murphey, Y.L.; Park, J.; Chen, Z.; Kuang, M.; Masrur, A.; Phillips, A. Intelligent hybrid vehicle power control—Part I: Machine learning of optimal vehicle power. *IEEE Trans. Veh. Technol.* **2012**, *61*, 3519–3530. [CrossRef]
20. Murphey, Y.L.; Park, J.; Kiliaris, L.; Kuang, M.; Masrur, A.; Phillips, A.; Wang, Q. Intelligent hybrid vehicle power control—Part II: Online intelligent energy management. *Trans. Veh. Technol.* **2013**, *62*, 69–79. [CrossRef]
21. Liu, Z.; Wang, D.; Jia, H.; Djilali, N.; Zhang, W. Aggregation and bidirectional charging power control of plug-in hybrid electric vehicles: Generation system adequacy analysis. *IEEE Trans. Sustain. Energy* **2015**, *6*, 325–335. [CrossRef]
22. Yilmaz, M.; Krein, P. Review of the impact of vehicle-to-grid technologies on distribution systems and utility interfaces. *IEEE Trans. Power Electron.* **2013**, *28*, 5673–5689. [CrossRef]
23. Singh, M.; Thirugnanam, K.; Kumar, P.; Kar, I. Real-time coordination of electric vehicles to support the grid at the distribution substation level. *IEEE Syst. J.* **2015**, *9*, 1000–1010. [CrossRef]
24. Haddadian, G.; Khalili, N.; Khodayar, M.; Shahidehpour, M. Optimal scheduling of distributed battery storage for enhancing the security and the economics of electric power systems with emission constraints. *Electr. Power Syst. Res.* **2015**, *124*, 152–159. [CrossRef]
25. Liu, H.; Hu, Z.; Song, Y.; Wang, J.; Xie, X. Vehicle-to-grid control for supplementary frequency regulation considering charging demands. *IEEE Trans. Power Syst.* **2015**, *30*, 3110–3119. [CrossRef]
26. Abdollah, K.F.; Rostami, M.A.; Niknam, T. Reliability-oriented reconfiguration of vehicle-to-grid networks. *IEEE Trans. Ind. Electron.* **2015**, *11*, 682–691. [CrossRef]
27. Kristien, C.N.; Haesen, E.; Driesen, J. The impact of charging plug-in hybrid electric vehicles on a residential distribution grid. *IEEE Trans. Power Syst.* **2010**, *25*, 371–380. [CrossRef]
28. Hoang, N.; Zhang, C.; Mahmud, M.A. Optimal coordination of *G2V* and *V2G* to support power grids with high penetration of renewable energy. *IEEE Trans. Transp. Electrification* **2015**, *1*, 188–195. [CrossRef]
29. Li, S.; Bao, K.; Fu, X.; Zheng, H. Energy management and control of electric vehicle charging stations. *Electr. Power Compon. Syst.* **2014**, *42*, 339–347. [CrossRef]
30. Omid, R.; Vafaeipour, M.; Omar, N.; Rosen, M.; Hegazy, O.; Timmermans, J.M.; Heibati, M.; Van Den Bossche, P. An optimal versatile control approach for plug-in electric vehicles to integrate renewable energy sources and smart grids. *Energy* **2017**, *134*. [CrossRef]
31. Bunyamin, Y.; Uzunoglu, M. A double-layer smart charging strategy of electric vehicles taking routing and charge scheduling into account. *Appl. Energy* **2016**, *167*, 407–419. [CrossRef]
32. Laiq, K.; Qamar, S. Online Adaptive Neuro-Fuzzy Based Full Car Suspension Control Strategy. In *Handbook of Research on Novel Soft Computing Intelligent Algorithms: Theory and Practical Applications*, 2nd ed.; Vasant, P., Ed.; IGI Global: Hershey, PA, USA, 2014; pp. 617–666, ISBN 9781466644502.
33. Thomas, B.; De Blasio, R. IEEE 1547 series of standards: Interconnection issues. *IEEE Trans Power Electron.* **2004**, *19*, 1159–1162. [CrossRef]